INDENTATION MODULUS AND YIELD POINT OF AU (111), (001), AND (110)

J. D. KIELY AND J. E. HOUSTON
Surface and Interface Sciences Department, MS 1413
Sandia National Laboratories, Albuquerque, NM 87185-1413

ABSTRACT

Nanoscale indentation experiments were performed on Au using the Interfacial Force Microscope (IFM) in an indentation mode. The indentation modulus and yield point were measured for three orientations of the Au surface: (111), (110), and (001). The indentation modulus for the (111) surface was found to be 36% greater than for the (001) surface and only 3% higher than the (110) surface. Additionally, the yield point was found to vary between orientations, but the shear stress resolved on {111} slip planes beneath the indenter on the axis of symmetry was found to be approximately 1.8 GPa for yield points of all three orientations.

INTRODUCTION AND EXPERIMENTAL PROCEDURE

Mechanical measurements were performed using the IFM. This instrument, which has been described in detail elsewhere [1], is distinguished by its use of a novel electrostatically-driven force-feedback system to ensure rigid displacement control during a loading experiment. Rigid displacement control ensures that instrument compliance (common in many indentation studies) does not exist, which simplifies analysis of elastic force profiles. Rigid displacement control is also advantageous when investigating the process by which materials plastically deform. Instabilities (e.g., jump-to-contact) are not present in this instrument and no energy is released from the sensor when a material's relaxation is plastic.

The indenters used in this study were electrochemically etched 100 μm tungsten wires with tip radii determined by field-emission scanning electron microscopy. Two tips were used in the modulus survey (750 Å and 1750 Å radii), while a number of tips were used in the yield point survey (1250 -1750 Å radii). Single-crystal Au samples with (001) and (110) surface orientations were Ar-ion sputtered and annealed at 950°C. The (111) surfaces were obtained by flame melting and annealing 99.99% pure Au wire to form a sphere with broad (111) facets [2, 3]. Immediately after cleaning, samples were immersed in a 0.5 mM ethanolic alkanethiol ($CH_3(CH_2)_{15}SH$) solution for 24 hr to develop a self-assembled monolayer (SAM) of hexadecanethiol to passivate the probe-sample interaction. Without the SAM, strong adhesive interaction occurs between the Au and W tip and the material is plastic on contact [4,5]. Passivation eliminates this adhesion [4,6] and allows us to analyze elastic force profiles using Hertzian theory [7,8], which predicts the elastic behavior of a parabolic tip and planar sample in the absence of adhesive or frictional interactions using continuum elasticity.

DISCLAIMER

RESULTS

By referring experimental results to the (111) orientation, we found that the indentation modulus for the (111) orientation was 36% greater than for the (001) orientation and that there was no statistically significant difference between (111) and (110) orientations. Figure 1 presents data from the three surfaces. Note the absence of any adhesive interaction and the Hertzian nature of the contact. From these data, we calculated the indentation modulus from Hertzian theory:

$$F = \frac{4}{3} E^* \sqrt{R}\, \delta^{3/2} \qquad (1)$$

where E* is the W - Au composite modulus, R is the tip radius, and δ is the depth of deformation. The results are presented in Table 1. The textbook value for polycrystalline Au is 78 GPa [9], which compares favorably with our measurements. Additionally, elastic constants for [111], [001], and [110] directions are 117, 43, and 82 GPa [9], which are reflected in the ordering of our results.

	E* (GPa)	E_{Au} (GPa)
(111)	79 ±1	78 ±1
(001)	62 ±4	57 ±3
(111)	85 ±7	85 ±7
(110)	83 ±7	82 ±6

Table 1. Composite moduli and Au indentation moduli measured from force profiles during retraction on Au (111), (001) and (110) surfaces. Two comparative experiments were performed using different tip-sensor combinations, resulting in different (111) moduli. Experimental uncertainty is that within one experiment (same tip and sensor).

Our results differ in some aspects from the predictions of Vlassak and Nix [10]. In their predictions for the effect of anisotropy on indentation, they predict that the indentation modulus for the (111) orientation will be 10% greater than that for the (001) orientation and 2% greater than that for the (110) orientation. We find the same order among orientations, but a greater variation between the (111) and (001) orientations (36 ± 11%). One difference between the two studies is that their predictions were developed for a rigid triangular punch while our indenter was an elastic paraboloid, but it is not clear how a change in indenter geometry results in different apparent moduli.

In addition to elastic properties, the stress required for plastic deformation was also measured as a function of orientation. Deviation from Hertzian behavior identifies the onset of plastic deformation. In some cases, this deviation was slight, but still identifiable, while in many cases, an abrupt and significant decrease in force identified the onset of plasticity. As an example of this abrupt onset of dislocation activity, Fig. 2 presents the response of a Au (001) crystal. Over the first 40-50 Å of deformation, the Au behaves elastically and, if the probe were to be removed, the force would decrease according to the Hertzian prediction. At a depth of approximately 50 Å and a force of approximately 14.5 μN, the measured force suddenly drops to 5 μN. As the probe continues to indent the sample, the force rises and drops as dislocation

activity continues. From the force (F), depth of deformation (δ), and tip radius (R), the mean applied stress normal to the surface at the initiation of dislocation activity may be calculated from the expression [7]

$$\bar{\sigma}_p = \frac{F_t}{\pi R \delta_t}, \tag{2}$$

where the subscript indicates the value at the plastic threshold. The mean plastic-threshold stress, whether it was in the form of a sudden drop in force or a more subtle deviation from elastic behavior, was found to be strongly dependent upon crystal orientation. The results are presented in Table 2.

Orientation	$\bar{\sigma}_p$ (GPa)
(001)	5.5 ±0.4
(111)	7.3 ±0.5
(110)	7.8 ±0.7

Table 2. Mean stress normal to the surface at the first deviation from Hertzian behavior.

In addition to stress at the yield point, the appearance of indentations varied with orientation. Fig. 3 demonstrates the strong effect crystal orientations has on indentation.

We have calculated {111}<110> shear stresses on the axis of symmetry and have determined the maximum value and the position at which it occurs. The results are presented in Table 3. Since the shear stress is given as a fraction of the mean applied stress, we can estimate the actual value of the maximum shear at the yield point (τ_c) from the measured applied mean stresses ($\bar{\sigma}_p$) listed in Table 2.

Orientation	Component	τ_c (GPa)
(001)	$(1\bar{1}\bar{1})[\bar{1}0\bar{1}]$	1.8 ± 0.1
(111)	$(1\bar{1}\bar{1})[\bar{1}0\bar{1}]$	1.7 ± 0.1
(110)	$(1\bar{1}\bar{1})[\bar{1}0\bar{1}]$	1.8 ± 0.2
(110)	$(\bar{1}\bar{1}1)[\bar{1}0\bar{1}]$	2.9 ± 0.3

Table 3. Maximum shear stress resolved in the direction of primary slip for three orientations of Au. Estimates of τ_c were obtained by multiplying the calculated maximum shear stress by measured $\bar{\sigma}_p$.

The most striking result of these estimates is that they demonstrate that τ_c is approximately equal on the $(1\bar{1}\bar{1})$ plane for each of the orientations. In other words, the Au lattice behaved elastically until τ_c reached 1.8 GPa on {111} planes. For the (110) orientation, two types of {111} planes exist and the shear stress on each type differs considerably at the yield point. This disparity between τ_c on {111} planes indicates that the yield condition for

nanoindentation may not be as simple as attaining a given yield stress (1.8 GPa in this case) on any slip plane, but on all slip planes. This implies that the geometry imposed by the indenter must be taken into account and that a sufficient number of slip systems must be activated to produce the observed deformation [11].

SUMMARY AND CONCLUSIONS

We have used the Interfacial Force Microscope to quantify the variation of indentation modulus and initial plastic yield stress with crystal orientation. Au single crystals with (001), (111) and (110) orientations were passivated with a self-assembling monolayer and probed using a parabolic W tip. By referring experimental results to the (111) orientation, we found that the indentation modulus for the (111) orientation was 36% greater than for the (001) orientation and that there was no statistically significant difference between (111) and (110) orientations. We showed that the initial yield point also varied considerably with orientation. The mean applied stress necessary to initiate plasticity was 5.5 GPa for (001)-oriented crystals, 7.3 GPa for (111)-oriented crystals and 7.8 GPa for (110)-oriented crystals. Assuming an isotropic Hertzian stress distribution, we have resolved maximum shear stresses on {111}<110> slip systems for each of the orientations and, by combining these predictions with known applied stresses, we have estimated the shear stress on {111}<110> slip systems at the initial yield point. The shear stress component on the $(1\bar{1}\bar{1})[\bar{1}0\bar{1}]$ slip system at the initial yield point was approximately 1.8 GPa for all three orientations. This suggests that 1.8 GPa is the critical resolved shear stress (CRSS) for creating a permanent indentation in Au, but since the processes by which dislocations nucleate, cross-slip and interfere during the formation of an indentation are unknown, it is unclear what process or processes the measured CRSS quantifies. It is clear, however, that performing indentation experiments on the nanometer level can provide information on material properties that are not dominated by pre-existing defects. It is also clear that these measurements, when considered in conjunction with theoretical modeling, can provide values for fundamental material parameters.

REFERENCES:

[1]. Michalske, T.A. and Houston, J.E., Acta Materialia **46**, 391-396 (1998).

[2]. Hsu, T. and Cowley, J.M., Ultramicroscopy **11**, 239 (1983).

[3]. Schneir, J., Sonnenfeld, R., Marti, O., Hansma, P.K., Demuth, J.E. and Hamers, R.J., J. Appl. Phys. **63**, 717-721 (1988).

[4]. Thomas, R.C., Houston, J.E., Michalske, T.A. and Crooks, R.M., Science **259**, 1883 (1993).

[5]. Houston, J.E., Michalske, T.A. and Crooks, R.M. Interfacial Adhesion at the Molecular Level in 20th Annual Meeting of the Adhesion Society. 1997. Hilton-Head, SC: The Adhesion Society.

[6]. Joyce, S.A., Thomas, R.C., Houston, J.E., Michalske, T.A. and Crooks, R.M., Physical Review Letters **69**, 2790-2793 (1992).

[7]. Johnson, K.L., Contact Mechanics. 1996, Cambridge: Cambridge University Press.

[8]. Timoshenko, S.P. and Goodier, J.N., Theory of Elasticity. 3rd ed. 1970, New York: McGraw-Hill.

[9]. Hertzberg, R.W., Deformation and Fracture of Engineering Materials. 1989, New York: John Wiley and Sons.
[10]. J.J. Vlassak and W.D. Nix, J. Mech. Phys. Solids **42**, 1223-1245 (1994).
[11]. J.D. Kiely and J.E. Houston, Phys. Rev. B **57** 12588 (1998).

ACKNOWLEDGMENTS

This work was supported by the U.S. Department of Energy under Contract DE-AC04-94AL85000. Sandia is a multiprogram laboratory operated by Sandia Corporation, a Lockheed-Martin Company, for the U.S. Department of Energy.

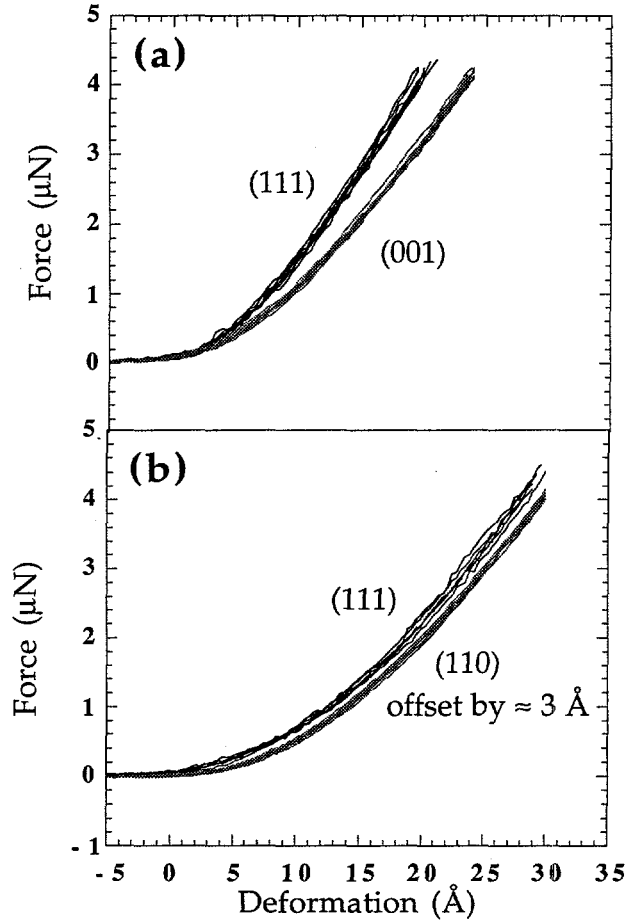

Figure 1. (a) Compiled retraction portion of loading cycles from (111)-oriented and (001)-oriented surfaces. The greater slope of the (111) force profiles indicates a higher indentation modulus. (b) Compiled retraction portion of loading cycles for (111)-oriented and (110)-oriented surfaces. The (110) force profiles have been offset by approximately 3 Å to distinguish the two data sets. The lack of any noticeable difference in the slopes indicates a difference in indentation modulus that is on the order of the scatter in measurement.

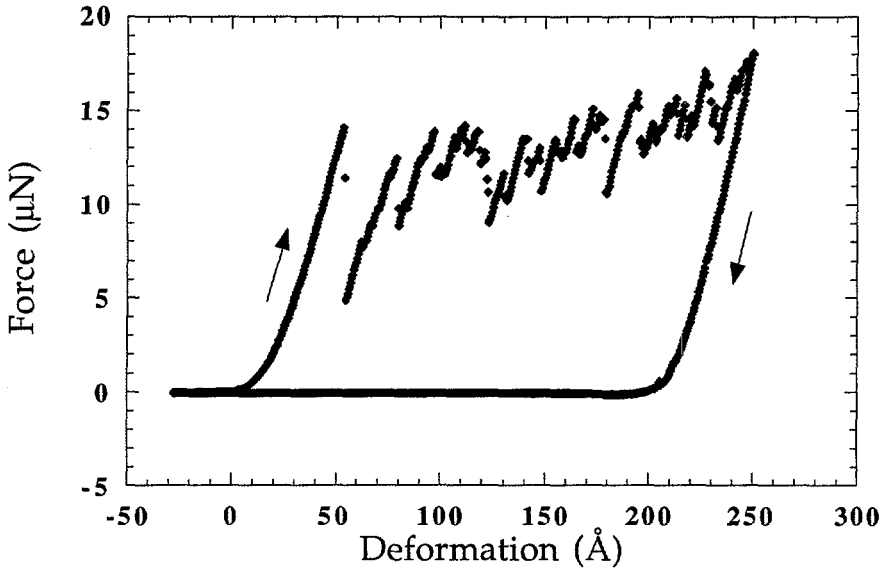

Figure 2. Loading cycle of a (111)-oriented surface when the elastic limit is surpassed. The initial ~50 Å of deformation is elastic and deviation from this Hertzian behavior identifies the initial yield point. Sudden force drops indicate dislocation activity, which continue until the probe is retracted. The width of the hysteresis loop, approximately 200 Å in this case, indicates the depth of the permanent indentation.

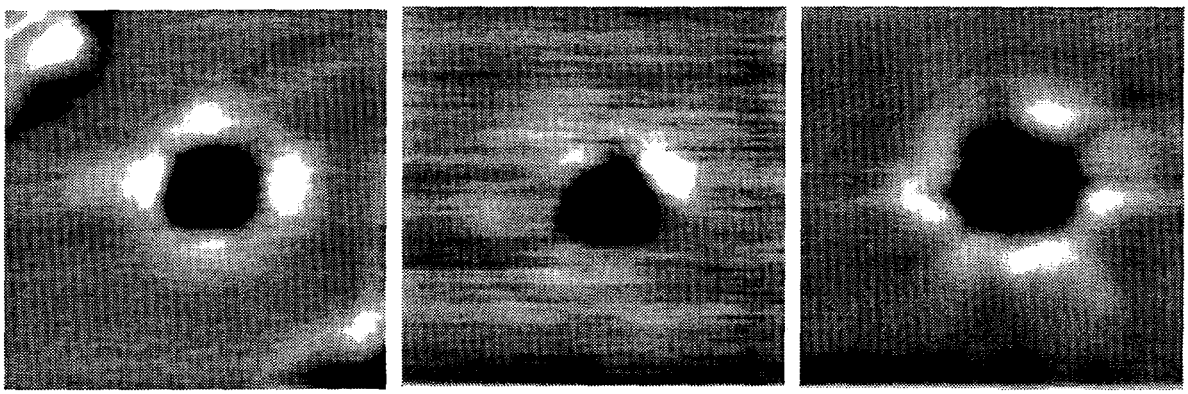

Figure 3. (a) Constant repulsive-force image (500 nm x 500 nm) of a permanent indentation on a (001)-oriented surface. The four-fold shape of the indentation and the four lobes of pile-up on the indentation periphery indicate the four-fold intersection of (111) slip planes with the surface. (b) A 300 nm x 300 nm image of a permanent indentation on a (111)-oriented surface. The triangular appearance of the indentation reveals the three-fold intersection of (111) slip planes with the surface. (c) A 300 nm x 300 nm image of a permanent indentation on a (110)-oriented surface. The indentation symmetry suggests that the orientation of (111) slip planes determines the structure of both the indentation and surrounding pile-up.